Acta Cryst. (1983). A**39**, 609–615

Dynamical Electron Diffraction from Elastically Bent Organic Crystals

BY BARBARA MOSS AND DOUGLAS L. DORSET

Medical Foundation of Buffalo, Inc., 73 High Street, Buffalo, NY 14203-1196, *USA*

(*Received* 16 *March* 1982; *accepted* 18 *August* 1982)

Abstract

Calculation of dynamical structure factors from a periodically curved crystal lattice have been carried out for the paraffin *n*-hexatriacontane, $C_{36}H_{74}$, and the linear polymer anhydrous nigeran, poly[(1→3)-α-D-maltose], $(C_{12}H_{20}O_{10})_n$. These are compared to dynamical structure factors from a flat crystal, and also to kinematic structure amplitudes from a bent lattice in order to determine the validity of considering each experimentally observed data perturbation separately. Individual treatment of these effects is found to be a good approximation so long as the crystal thickness and bend deformations are each small.

Introduction

Of the possible data perturbations which may offset the success of quantitative *ab initio* crystal-structure analysis of organic materials from electron diffraction intensities, two have been identified to be the most significant. The existence of dynamical scattering, which has been confirmed in at least four separate experimental ways (Dorset, 1976*a*,*b*, 1980) becomes most problematic for light-atom structures as crystal thickness increases or as the incident electron beam energy is decreased; this is consistent with theory (*e.g.* Cowley, 1975). With proper control of thickness and incident beam wavelength, the influence of this perturbation can be made small enough to allow structure analysis by conventional crystallographic techniques such as 'direct phasing' (Dorset, Jap, Ho & Glaeser, 1979).

The second important data perturbation, which has also been largely ignored, is the influence of omnipresent elastic crystal bends on the diffraction intensities (Cowley, 1961). Such effects are quite significant for many organic materials since the longest unit-cell axis is posited by solution crystal growth to lie approximately parallel to the incident electron beam direction. This has been experimentally verified for several representative paraffins and paraffin derivatives (Dorset, 1978, 1980) as well as for some linear polymers (Dorset & Moss, 1981; Moss & Dorset, 1982*a*). The success of phasing procedures for the derivation of a correct crystal structure is dependent upon unit-cell axial length in the beam direction and the amount of crystal bend deformation (Moss & Dorset, 1982*b*). It is seen that if a unit-cell axis is particularly long, a correct crystal structure may not be obtainable from solution-grown crystals, necessitating epitaxial growth techniques to ensure a small cell axis to parallel the beam direction (Dorset, 1980).

Although the influences of these two data perturbations have been separately identified and accounted for it is desirable to combine them in a single calculation. Previous treatment of electron diffraction data from representative polymer structures (Moss & Dorset, 1982*a*) has revealed instances where one or the other is most important for the verification of a structural model. Thus a combined treatment of their effects will indicate the appropriateness of these separate corrections.

In this paper we demonstrate such a combined treatment with multislice dynamical calculations for curved crystal lattices by considering two representative structures, the paraffin *n*-hexatriacontane and the linear polymer nigeran. Preliminary results have been reported previously (Moss & Dorset, 1981).

Structures

Hexatriacontane

Hexatriacontane, $C_{36}H_{74}$, is a long-chain hydrocarbon which crystallizes from solution with the long ($c = 95{\cdot}14$ Å) axis parallel to the electron beam (Teare, 1959). In this projection down the chain axis there is also a methylene 'subcell' of length 2·54 Å due to the carbon zig-zag repeat. Dynamical effects are apparent for a crystal of monomolecular thickness (one-half unit cell) (Dorset, 1976*a*,*b*), and the large projection axis for the total unit cell enhances any crystal bending effects. It is thus a particularly difficult structure to analyze totally from *hk*0 electron diffraction data. Crystallographic details are given in Table 1 and the structure is illustrated in Fig. 1.

0108-7673/83/050609-07$01.50

Anhydrous nigeran

Nigeran crystallizes from solution with a 14·62 Å axis in the electron beam direction (Pérez, Roux, Revol & Marchessault, 1979). Comparison of dynamical perfect-crystal calculations and kinematical bent-crystal calculations with extensive experimental data indicates that both these effects are relatively unimportant in thin specimens (Moss & Dorset, 1982*a*). Crystallographic data are summarized in Table 2, and Fig. 2 shows a view of the structure.

Calculations

(i) *Kinematical.* Applications of Cowley's kinematical model for diffraction from bent crystals have been described elsewhere (Dorset, 1978, 1980; Moss & Dorset, 1982*b*). Diffracted beam intensities are calculated with a Patterson function, for which the peaks have been smeared out to account for the bending. For zones where the projection is down a long crystallographic axis intensities are severely affected by small amounts of bend, giving an effective coherence restriction in the beam direction. Zones projecting down a small axis are less sensitive. In the expression for the diffracted beam intensity the term describing the bending has an exponential form and its neglect may sometimes lead to the use of unrealistically low temperature factors for electron diffraction data (Moss & Dorset, 1982*a*).

(ii) *Dynamical.* In analogy with the treatment of defect structures (Fields & Cowley, 1978) an artificial superlattice is constructed, containing several unit cells arranged to model a deformed foil. This is the basic structure unit for the dynamical structure factor calculation. The method of periodic continuation (Grinton & Cowley, 1971) is employed. The new structural unit, convoluted with superlattice vectors in the plane perpendicular to the incident beam direction, forms a superlattice slice of the deformed structure, which is input to the *n*-beam multislice programs. The use of a large superlattice results in a very large number of diffracted beams; those beams corresponding to the original unit cell contain information on the average structure while the effect of the deformation is included in the additional beams representing the diffuse scattering. After being dynamically scattered through the required crystal thickness the diffracted beam amplitudes corresponding to the original unit cell are examined. This is equivalent to taking the peak height rather than the integrated intensity of the smeared Bragg peak. For most of the beams considered the smeared density falls off rather sharply and regularly around the Bragg peak. The sinusoidal deformation utilized cannot explain the considerable continuous diffuse scattered intensity which is experimentally observed between the 200 and 110 Bragg reflections (Dorset, 1977).

Table 1. *Orthorhombic hexatriacontane* $C_{36}H_{74}$ *crystal structure* (*Teare,* 1959)

Space group $Pca2_1$
Lattice parameters $a = 7{\cdot}42$ (1) Å
$b = 4{\cdot}96$ (1) Å
$c = 95{\cdot}14$ (20) Å
4 molecules per unit cell

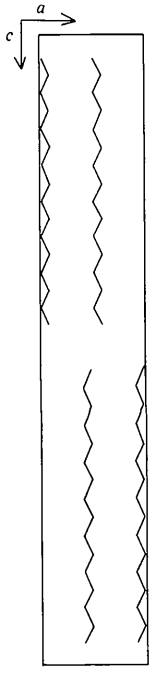

Fig. 1. Projection of a typical orthorhombic paraffin crystal structure along the *b* axis, after Teare (1959).

Table 2. *Anhydrous nigeran, poly*[(1→3)-α-D-*maltose*], *crystal structure* (*Pérez, Roux, Revol & Marchessault,* 1979).

Space group $P2_12_12_1$
Lattice parameters $a = 17{\cdot}76$ Å
$b = 6{\cdot}0$ Å
$c = 14{\cdot}62$ (Å) (fiber repeat)
4 molecules per unit cell

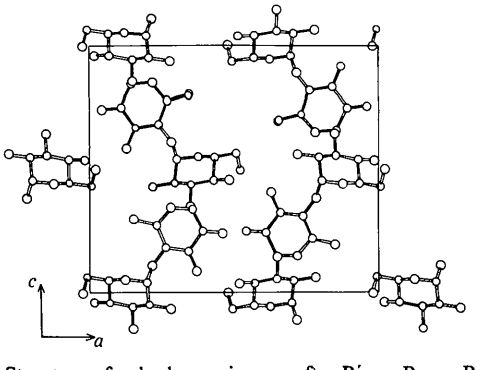

Fig. 2. Structure of anhydrous nigeran, after Pérez, Roux, Revol & Marchessault (1979).

For a uniformly-bent foil it is possible, in kinematical diffraction theory, to relate the radius of curvature of the specimen (R) to the distance between bend contours due to a reflection and its Friedel pair (S) (see Fig. 3). For a regular cylindrically bent crystal,

$$R = S/2\theta_B,$$

where θ_B is the Bragg angle. The amount of bend, α, is given by D/R with D the distance between sets of bend contours due to the same reflection (see Fig. 4).

Here the distorted foil is represented by a sine function in two dimensions. The basic repeat unit is a supercell composed of $n \times m$ unit cells displaced vertically in the beam direction **c** and rotated according to the amplitude and gradient of the sine functions. With a one-dimensional sine function

$$\mathbf{z} = A \sin(t\mathbf{x}),$$

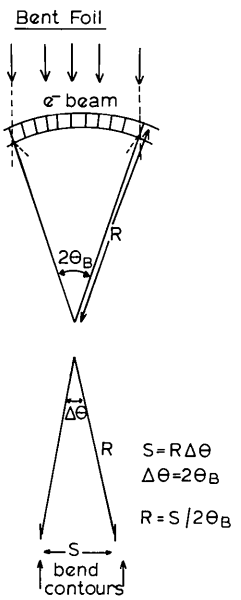

Fig. 3. Diagram showing Bragg diffraction from a bent foil and the resultant bend contours, arising from diffraction planes at correct angle to the incident beam.

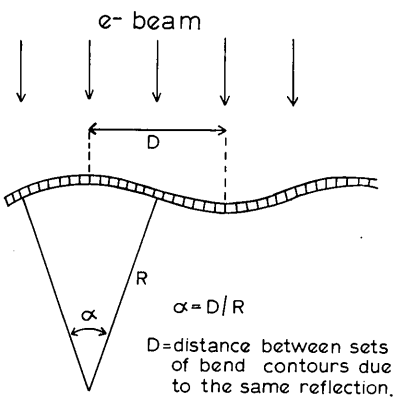

Fig. 4. Model of a foil periodically deformed in one dimension.

and approximating the sine curve as spherical (as in Fig. 4) the experimentally measurable parameters D and R can be related to those modeling the distortions:

$$t = \pi/D$$

$$A = R \pm (R^2 - \pi^2/4t^2)^{1/2}.$$

The first distortion considered was one-dimensional, along the **b** axis, giving the new supercell dimension $\mathbf{b}' = n\mathbf{b}$. Each original unit cell is displaced in the beam direction according to the amplitude of the sine function at that point and rotated about an axis in the direction $\mathbf{b} \times \mathbf{c}$ by an amount φ, where $\tan\varphi$ is the gradient of the sine function at that point. Subsequently, a sine distortion is applied along the **a** axis, where the new supercell dimension is $\mathbf{a}' = m\mathbf{a}$. The basic unit cells are further displaced vertically, and rotated about an axis in the direction $\mathbf{a} \times \mathbf{c}$ according to the amplitude and gradient of this second modulation function. Values of n,m, displacements and rotation angles for different amounts of bend are given in Table 3 for both structures. The model is somewhat unrealistic as the radii of curvature employed, of the order of a few hundred ångströms, are comparable to the lateral coherence range of the incident beam under normal operations. From experimental measurements of bend contour spacings the radii of curvature are typically much larger than the lateral coherence range. A larger radius of curvature, and supercell dimension, will result in finer sampling of the diffuse scattering in the resultant diffraction pattern but the Bragg peaks should not be greatly altered. However, any realistic image calculation of a deformed foil would require that the supercell dimensions (and thus the radius of curvature) are larger than the lateral coherence if the artificial periodicity of the model is not to be transferred to the calculated image.

For both hexatriacontane and nigeran, hydrogen atoms are neglected and a Debye–Waller temperature factor of 6 Å^2 is applied. With the supercell model a large number of Fourier coefficients are required to describe the structure and to determine the resulting diffracted beam amplitudes. Our present maximum is 4000 beams, which limits the resolution of the resultant

Table 3. *Parameters for bent supercell*

Structure	n	m	Bend angle (°)	A_x (Å)	A_y (Å)	φ_{max} (°)
Hexatriacontane	10	8	2·5	0·16	0·14	0·93
			5·0	0·32	0·27	1·87
Nigeran	10	5	2·0	0·20	0·13	0·74
			5·0	0·49	0·33	1·88

The supercell lattice parameters are $\mathbf{a}' = m\mathbf{a}$, $\mathbf{b}' = n\mathbf{b}$, $c' = \mathbf{c}$. A_x and A_y are respectively the amplitudes of the sine distortion in the **x** and **y** directions. φ is the angle of rotation of an individual unit cell in the supercell.

supercell data to $d^*_{max} = 0{\cdot}49$ Å^{-1} for nigeran, and $d^*_{max} = 0{\cdot}66$ Å^{-1} for hexatriacontane. Diffracted beams near this limit will have the largest errors but the calculations should be useful in obtaining approximate structure amplitudes for the strong low-order beams. The slice thicknesses used are respectively 3·655 and 2·973 Å for nigeran and hexatriacontane. No absorption is included and 100 kV electrons are assumed. In all cases over 99% of the energy is retained at the end of the multislice calculations.

Results

(i) *Hexatriacontane.* After one unit-cell thickness, dynamical scattering results in the breakdown of Friedel's law – even for the flat crystal case. For the ten lowest-angle reflections, the average deviation from the mean of $|F_{hk0}|$ and $|F_{\bar{h}\bar{k}0}|$ varies as a function of bend angle, but is always greater than 10%. Dynamical scattering also results in the F_{0k0} reflections with $k = 2n + 1$ having small non-zero intensities. Introduction of crystal bending additionally gives rise to non-zero intensities for the F_{h00}, $h = 2n + 1$, reflections (which are symmetry forbidden in kinematic theory).

For each bend angle, reflections corresponding to the eleven lowest-angle reflections of the original unit cell have been normalized to have the same $\sum F^2_{hk0}$, and plotted for the kinematical and the dynamical supercell calculations in Figs. 5(*a*) and (*b*). Apart from the 7·5° bend results, the relative intensities of the two strongest beams, the 110 and the 200 give a very good indication of the bend angle, with the kinematical value implying the same degree of bend as the more complete dynamical treatment. The behavior of the two data sets is quite similar, with most reflections following nearly the same function with bend for the different calculations.

Given this close agreement, we feel that the use of the kinematical treatment, which is considerably easier and quicker to carry out than the supercell calculation, is a good approximation in this case.

(ii) *Nigeran.* As the microcrystals may be of varying thickness, diffracted beam amplitudes for crystals up to ten unit cells (146·20 Å) have been calculated by the supercell approach. Again, all data sets, composed of the nineteen lowest-angle reflections of the original unit cell, are normalized to have the same $\sum F^2_{hk0}$. Fig. 6 shows magnitude variations of the 200, 020 and 110 reflections with increasing thickness. The kinematical values are also indicated. Each reflection exhibits the same form of thickness dependence for the different bends, although the magnitudes differ by up to 15%. The trend in amplitudes agrees with that shown by the respective kinematic values, except for the reversal of the 2 and 5° results for the 020 reflection. Thus the kinematical values are generally quite good approximations to the average dynamical values over the range of crystal thicknesses of interest.

Fig. 7 gives the variation of diffracted beam amplitudes as a function of bend angles at thicknesses of one and ten unit cells. For comparison the kinematical bend results (which are independent of thickness) are shown in Fig. 8. With changes of crystal thickness the behavior of the dynamically scattered beams is different, with those for the thinnest crystal most closely resembling the kinematical result. At a

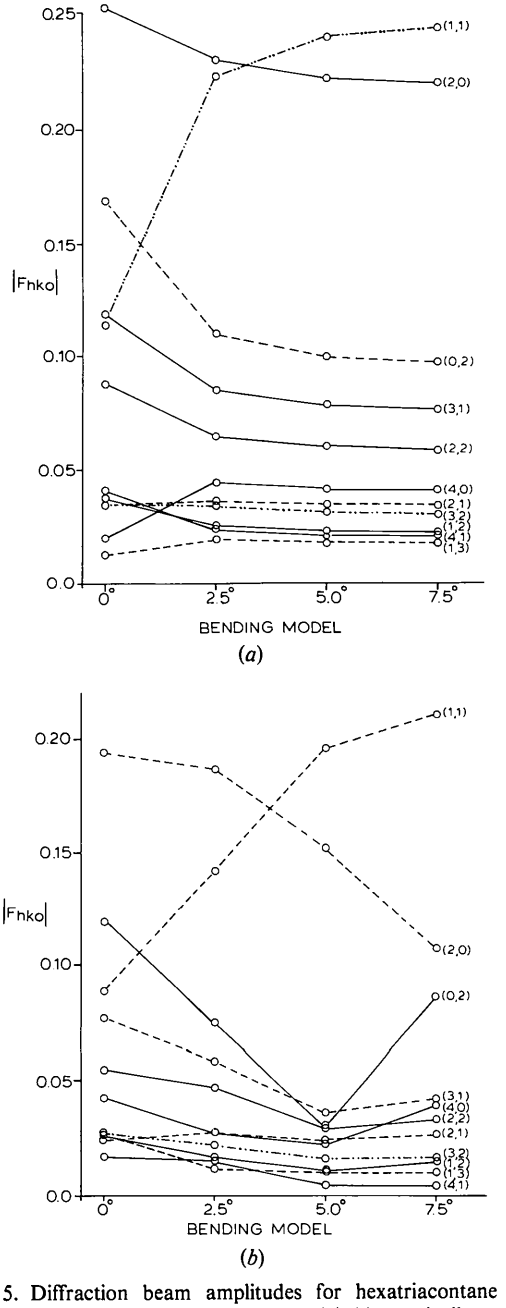

Fig. 5. Diffraction beam amplitudes for hexatriacontane as a function of bend angles calculated (*a*) kinematically and (*b*) dynamically.

thickness of ten unit cells the 200 is the strongest reflection, rather than the 020. With increasing crystal thickness, the ordering of normalized structure amplitudes from strongest to weakest differs markedly from the kinematic result. At the resolution considered the Patterson maps for a crystal five unit cells thick, both flat and with 5° bend, are extremely similar to the ideal flat kinematical result.

The dynamical intensity data have been compared with experimental electron diffraction data obtained by Pérez *et al.* (1979). The experimental amplitudes form a more extensive set than those calculated, extending to $d^*_{max} = 0{\cdot}78$ Å^{-1}, from crystals estimated to be 90 Å thick. Of these, the nineteen lowest-order reflections were normalized as before and compared to the various dynamical amplitudes. As Fig. 9 indicates, the 0 and 2° bend cases have minimum agreement factors at a crystal thickness of four unit cells (58 Å) while the 5° bend calculation gives closest agreement as the crystal thickness tends to zero. The differences among all these results are very small. For a physically reasonable interpretation we expect a minimum R factor at a finite crystal thickness. Thus the 2° bending model seems the most appropriate. For comparison, a purely kinematical calculation gives best agreement with the same set of reflections ($R = 0{\cdot}18$) for 1° crystal bending, close to the dynamical result.

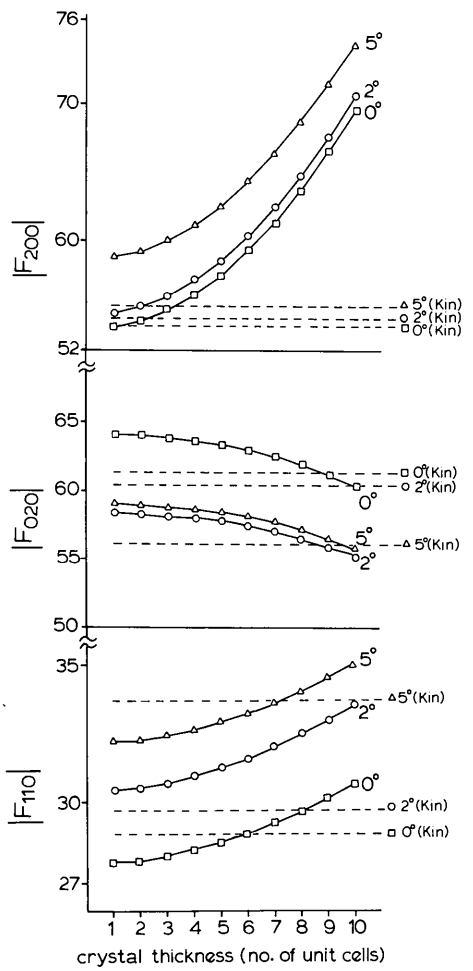

Fig. 6. Representative dynamical diffracted beam amplitudes (full lines) for nigeran as a function of crystal thickness and bend angle. The kinematic values are shown as broken lines. (*a*) 200, (*b*) 020 and (*c*) 110 reflection.

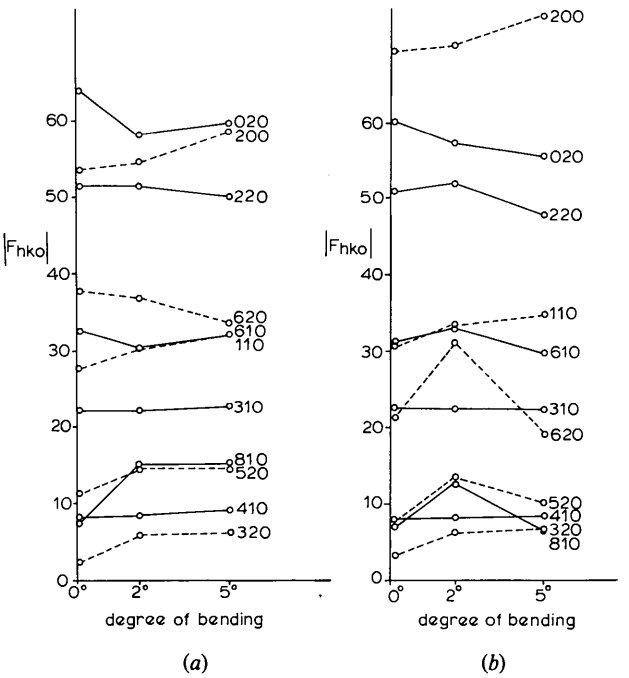

Fig. 7. Dynamical diffracted beam amplitudes for nigeran for different bend angles at crystal thicknesses of (*a*) one unit cell (14·62 Å) and (*b*) ten unit cells (146·20 Å).

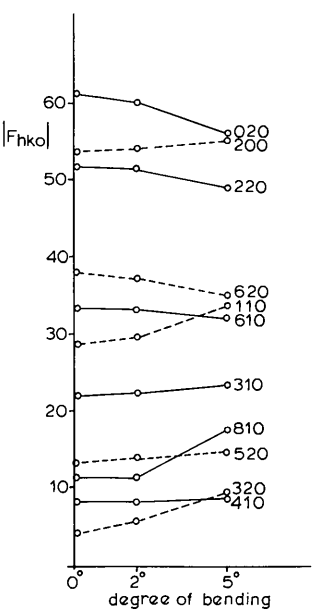

Fig. 8. Kinematic structure amplitudes for nigeran as a function of bend angle.

Discussion

It is apparent from the above analysis that the separate treatment of dynamical effects and elastic bending for organic crystals is usually an adequate approximation. The diffraction amplitudes generated with the sine distortion model considered above provide a suitable description for the two structures considered. For extremely thin crystals, the change in diffraction amplitudes with bending closely resembles kinematical predictions. For thicker crystals the dynamical effects are more pronounced. In general the changes in diffraction amplitudes with crystal thickness show the same trend found for a perfectly flat plate. It is fortunate that separation of these calculations can be justified, for a more accurate supercell treatment including a more realistic crystal radius of curvature and a finer sampling of crystal potential may require prohibitive computing time. [Spence (1978) has discussed some judicious approximations which could reduce the calculation time.]

With the recognition of their influence and importance, it is apparent that the two perturbations must be experimentally diminished *a priori* to ensure the success of crystal structure analysis. Minimization of crystal thickness and therefore *n*-beam scattering contributions appears to be easier for some materials than others. Linear polymers, for example, often give suitably thin monolamellae from solution which accounts for the relatively large number of such crystal structures solved with the use of electron diffraction data. For other materials, *e.g.* amino acids, small polar aromatics, *etc.*, which are stabilized by hydrogen bonding, the crystal growth appears to be more difficult to control and this may account for the difficulties in pioneering structure determinations from electron diffraction data (*e.g.* Lobachev & Vainshtein, 1961). Along with the enhanced presence of *n*-beam dynamical interactions at greater crystal thickness comes the more difficult-to-treat multiple incoherent scattering contribution (Cowley, Rees & Spink, 1951).

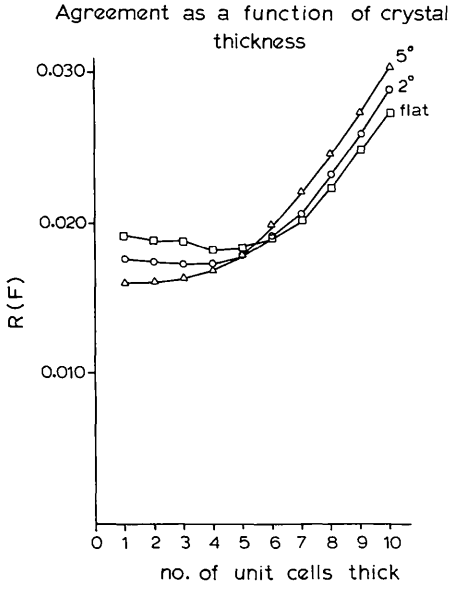

Fig. 9. Crystallographic residual, $R(F)$, comparing experiment (Pérez, Roux, Revol & Marchessault, 1979) and calculation for the 19 lowest-angle reflections of nigeran, as a function of crystal thickness.

Long unit-cell axes can be forced to lie perpendicular to the incident beam by epitaxy – thus minimizing the effects of elastic bending. This has been demonstrated for paraffins (Wittmann & Manley, 1978), linear polymers (Wittmann & Manley, 1977) and aromatics (Uyeda, Kobayashi, Suito, Harada & Watanabe, 1972; Fryer, 1978). The control of crystal thickness, moreover, seems to be most easily affected when the material is sublimed onto a nucleating substrate (Kobayashi, Fujiyoshi, Iwatsu & Uyeda, 1981). When a suitably short unit cell lies parallel to the incident electron beam, the electron diffraction data represent the total projected crystal structure (Dorset, 1980).

Although procedures for optimal electron diffraction data collection differ in concept from those required for X-ray or neutron experiments, there is now ample evidence that *ab initio* structure analysis is attainable and believable. While 'molecular' electron images of radiation-stable (or -stabilized) organics give useful information, *e.g.* on crystal defect structures, there is much higher atomic resolution information which can be obtained from the diffraction intensities by this 'crystallographic' approach. At present this approach is needlessly under-utilized.

We thank Dr John Spence of Arizona State University for enlightening discussions. Financial support from the National Science Foundation through grants CHE79-16915 and CHE81-16318 is gratefully acknowledged.

References

Cowley, J. M. (1961). *Acta Cryst.* **14**, 920–927.
Cowley, J. M. (1975). *Diffraction Physics*. Amsterdam: North-Holland.
Cowley, J. M., Rees, A. L. & Spink, J. A. (1951). *Proc. Phys. Soc. London Sect. A*, **64**, 609–619.
Dorset, D. L. (1976*a*). *Acta Cryst.* A**32**, 207–215.
Dorset, D. L. (1976*b*). *J. Appl. Phys.* **47**, 780–782.
Dorset, D. L. (1977). *Z. Naturforsch. Teil A*, **32**, 1161–1165.
Dorset, D. L. (1978). *Z. Naturforsch. Teil A*, **33**, 964–982.
Dorset, D. L. (1980). *Acta Cryst.* A**36**, 592–600.
Dorset, D. L., Jap, B., Ho, M. & Glaeser, R. M. (1979). *Acta Cryst.* A**35**, 1001–1009.
Dorset, D. L. & Moss, B. (1981). *ACS Polym. Preprints*, **22**, 267.
Fields, P. M. & Cowley, J. M. (1978). *Acta Cryst.* A**34**, 103–112.
Fryer, J. R. (1978). *Acta Cryst.* A**34**, 603–607.
Grinton, G. R. & Cowley, J. M. (1981). *Optik (Stuttgart)*, **34**, 221–232.

KOBAYASHI, T., FUJIYOSHI, Y., IWATSU, F. & UYEDA, N. (1981). *Acta Cryst.* A**37**, 692–697.
LOBACHEV, A. N. & VAINSHTEIN, B. K. (1961). *Sov. Phys. Crystallogr.* **6**, 313–317.
MOSS, B. & DORSET, D. L. (1981). *Proc. 39th Ann. Meeting Electron Microscopy Soc. of America*, pp. 344–345. Baton Rouge, Louisiana: Claitor.
MOSS, B. & DORSET, D. L. (1982*a*). *J. Polym. Sci. – Polym. Phys. Ed.* **20**, 1789–1804.
MOSS, B. & DORSET, D. L. (1982*b*). *Acta. Cryst.* A**38**, 207–211.
PÉREZ, S., ROUX, M., REVOL, J. F. & MARCHESSAULT, R. H. (1979). *J. Mol. Biol.* **129**, 113–133.
SPENCE, J. C. H. (1978). *Acta Cryst.* A**34**, 112–116.
TEARE, P. W. (1959). *Acta Cryst.* **12**, 294–300.
UYEDA, N., KOBAYASHI, T., SUITO, E., HARADA, Y. & WATANABE, M. (1977). *J. Appl. Phys.* **43**, 5181–5189.
WITTMANN, J. C. & MANLEY, R. ST JOHN (1977). *J. Polym. Sci. – Polym. Phys. Ed.* **15**, 1089–1100.
WITTMANN, J. C. & MANLEY, R. ST JOHN (1978). *J. Polym. Sci. – Polym. Phys. Ed.* **16**, 1891–1895.

Acta Cryst. (1983). A**39**, 615–621

Moments of the Trigonometric Structure Factor

BY URI SHMUELI AND UZI KALDOR

Department of Chemistry, Tel-Aviv University, 69 978 Ramat Aviv, Israel

(*Received* 1 *July* 1982; *accepted* 9 *March* 1983)

Abstract

The eighth moment of the magnitude of the trigonometric structure factor has been computed for all the space groups and all the reflection subsets giving rise to different functional forms of this quantity. This extension of previously published computations of lower moments permits the construction of four-term generalized distributions of normalized intensity, which are necessary in treating problems arising from highly heterogeneous atomic compositions in various space-group symmetries. The related problem of odd–even mixed partial moments of the trigonometric structure factor has also been investigated, and these mixed moments were found to vanish for all the three-dimensional space groups, confirming the correctness of the hitherto published theoretical statistics. Similar computations for the plane groups showed that non-zero values of the mixed partial odd–even moments are obtained for *p*3, *p*31*m*, *p*3*m*1, *p*6 and *p*6*m*. This result calls for some modifications of the statistical formalism to be applied to two-dimensional sets of intensity data. The modifications required for the centrosymmetric case are indicated in some detail.

Introduction

Statistical treatments of distributions of the diffracted intensity range from the use of asymptotic distributions based on the central-limit theorem (*e.g.* Cramér, 1951, p. 214) to applications of generalized expansions, associated with such asymptotic probability functions. The latter include the well known centric and acentric Wilson (1949) distributions, as well as a few others which allow for hypersymmetry (Rogers & Wilson, 1953), partial centrosymmetry (Srinivasan & Parthasarathy, 1976) and dispersion (Wilson, 1980). Generalizations of the above consist of expansions in terms of orthogonal polynomials with coefficients depending explicitly on the space-group symmetry, number of atoms in the unit cell and their scattering powers (*e.g.* Hauptman & Karle, 1953; Bertaut, 1955; Klug, 1958; Shmueli, 1979; Shmueli & Wilson, 1981, 1983; Shmueli, 1982*a*). The dependence on symmetry enters the formalisms *via* mean values of powers of trigonometric structure-factor moduli and the computation of these mean values, or moments, is a prerequisite for any practical application of these generalized statistics. The first extensive calculation of this kind was carried out by Wilson (1978) who found the fourth moment of the trigonometric structure factor for all the space groups but two (*Fd*3*m* and *Fd*3*c*). Similar straightforward calculations of moments higher than the fourth proved impracticably cumbersome and error-prone, and two computer programs were developed whereby the fourth and sixth moments have been obtained for all the space groups and all the reflection subsets that give rise to different functional forms of the structure factor (Shmueli & Kaldor, 1981). Since moments up to and including the 2*n*th are required for *n*-term expansions (*cf.* Shmueli & Wilson, 1981) the above computations led to generally usable three-term distributions. However, simulated distributions (Shmueli, 1982*b*), as well as those recalculated from published structures of several organometallic compounds (Shmueli, 1982*a*), show clearly that for extreme atomic heterogeneities (*e.g.* a platinum among fifteen light non-H atoms), still encountered in practical work, at least four-term generalized expansions are

0108-7673/83/050615-07$01.50